

High-resolution observations on fine-scale spatial and temporal heterogeneity of phytoplankton communities using FlowCAM

KHIN KHIN GYI¹⁾, Takuo OMURA^{2, 3)}*, Rie NAKAMURA³⁾ and Yuji TANAKA^{1, 2)}

Abstract: To understand the fine-scale spatio-temporal phytoplankton dynamics with reference to the environmental properties of the water column, high-frequency samplings every 4 h, at 0.5–2 m depth intervals using a submersible pump was conducted in Tateyama Bay, Japan, for 24 h from 12 h of 12 May to 08 h of 13 May 2017. The FlowCAM, which is an automatic device, was used to identify, count and size the phytoplankton. As a result, the phytoplankton distribution significantly varied within a few meters and a short timescale (several hours) of a day. For example, *Thalassiosira* sp. and *Prorocentrum minimum* were detected at all sampling depths and times rather evenly, but the water-column total abundance of *Dactyliosolen fragilissimus* and *Scrippsiella trochoidea* significantly decreased after the 2nd set of the samplings. Species-specific vertical distributions were various but related to the condition (strength and depth) of the thermocline at each sampling time. These phytoplankton species-specific distributions and variations in the composition reflect the eco-physiological characteristics and size structure of phytoplankton and the short-term hydrodynamic events. The high value of chlorophyll-*a* in the bottom layers was not only from the phytoplankton but also from the fluorescence of the aggregate particles.

Keywords : *phytoplankton, spatio-temporal distribution, FlowCAM, fine-scale sampling*

1) Graduate School of Marine Science and Technology, Tokyo University of Marine Science and Technology, 4-5-7 Konan, Minato, Tokyo 108-8477, Japan

2) Department of Ocean Sciences, School of Marine Resources and Environment, Tokyo University of Marine Science and Technology, 4-5-7 Konan, Minato, Tokyo 108-8477, Japan

3) Laboratory of Aquatic Science Consultant, 2-30-17 Higashikamata, Ota, Tokyo 144-0031, Japan

*Corresponding author: Takuo OMURA

Tel: 03-6428-6715

Fax: 03-6428-6716

E-mail: omura@lasc.co.jp

1. Introduction

The vertical distribution of phytoplankton community in the water column is highly heterogeneous in response to the small-scale physical hydrodynamic changes such as water mass stability (MELLARD *et al.*, 2011), vertical mixing (MAZNAH *et al.*, 2016), and the availability of light (TILZER and GOLDMAN, 1978). Variations of the abiotic water conditions occur naturally at different timescales throughout the day (GAST *et al.*, 2014), related with the periodic oscillations of the tidal currents (BLAUW *et al.*, 2012), which in turn influence the short-term changes in the phytoplankton community.

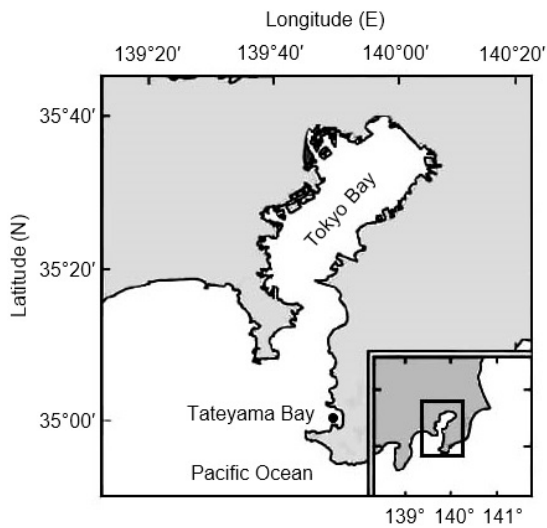


Fig. 1 The sampling site (solid circle) in Tateyama Bay, Japan.

Despite the relationship between environmental properties, ecological characteristics and fine-scale phytoplankton dynamics has been reported by previous studies (*e.g.* DEKSHENIEKS *et al.*, 2001; GERVAIS *et al.*, 2003; LUNVEN *et al.*, 2005; CARON *et al.*, 2008), it is still remaining to explore how do phytoplankton fluctuate throughout the entire water column, in a short timescale of the day. Hence, we here conducted a series of pump samplings throughout the whole vertical water column, at a relatively fine-scale of 0.5–2 m depth interval, every 4 h, dealing with the physical characteristics of the water column. The aim was to understand the precise spatial and temporal distributions of phytoplankton abundance, composition and the size structure, together with the particle distribution data, and thus provide relevant information about the short-term changes in the phytoplankton vertical distribution and the community dynamics. In the case of monitoring the high-resolution field survey data, traditional microscopic examination is time-consuming. To overcome this difficulty, we de-

ployed an automatic device FlowCAM (the Flow Cytometer And Microscope), which has combined capabilities of flow cytometry, microscopy and image analysis (SIERACKI *et al.*, 1998). This apparatus counts and photographs particles moving in a fluid flow. To create this flow, the water sample is drawn into the instrument by means of a peristaltic pump. A digital camera photographs the particles as they pass through a prismatic glass chamber mounted on a cell holder in front of a microscope lens (POULTON and MARTIN, 2010). The FlowCAM provides informative information for plankton study as follows: (1) cell counts and sizing accuracy (SIERACKI, *et al.*, 1998; SEE *et al.*, 2005; TAUXE *et al.*, 2006; ÁLVAREZ *et al.*, 2014), and (2) high-quality images for species identification as a VisualSpreadsheets (CAMOYING and YÑIGUEZ, 2016). Taking these advantages of FlowCAM, we can reduce the time for sample processing and increase the resolution of the field survey.

2. Materials and methods

2.1 Sampling site and sample collection

The sampling was carried out onboard a training ship *Seiyo-maru* of Tokyo University of Marine Science and Technology anchored at a point of 23 m deep in Tateyama Bay (35°00.06' N, 139°49.87' E), Japan (Fig. 1). On 12–13 May 2017, a total of six samplings were conducted every 4 h at 12, 16, 20, 00, 04 and 08 h (JST). Water samples were obtained using a vortex submersible pump (pumping speed: 0.5 m³ min⁻¹) following the method of ITOH *et al.* (2011), which is originally consulting the depth discrete pump sampling system shown in HARRIS *et al.* (1986). The depth interval was set every 0.5 m from 0 to 14 m, and 2 m from 16 to 20 m depth. We collected 192 samples in total, from 32 distinct vertical water layers within 0–20 m depth. For the phytoplankton analysis, water samples of 500 mL

were collected and immediately fixed with formalin (final concentration 1%). Concurrently, vertical profiles of water temperature, salinity, and density (σ_t) were taken using a CTD (AAQ-RINKO, JFE Advantech, Co., Ltd., Tokyo, Japan) fitted with an *in vivo* chlorophyll-*a* fluorescence sensor, a nephelometric sensor, and photosynthetically active radiation (PAR) sensor. At each time, a series of pump sampling was completed within about an hour.

Sunrise and sunset were at 04:39 and 18:34, on the sampling days. The first day (May 12) was calm and sunny while the second day (May 13) was quite windy and rainy. Information about the tide level of the sampling area was obtained from the Japan Meteorological Agency website (http://www.data.jma.go.jp/kaiyou/data/db/tide/suisan/pdf_hourly/2017/TT.pdf). Two low tides and two high tides were included during the sampling period (Fig. 2).

2.2 Phytoplankton and aggregate particle analyses by the FlowCAM

Phytoplankton samples were counted in triplicate using the automatic sample analysis device, FlowCAM (Fluid Imaging Technologies, Inc., ME, USA). In this study, particle images were captured by the FlowCAM auto-image mode, with an imaging rate of 5 frames per second, the FC100 flow cell (100 μm chamber depth) and the 10 x objective lens. The flow rate was controlled by the rotation rate of the pump (0.14 mL min^{-1}). Phytoplankton were identified by visual inspection using the image analysis software (VisualSpreadsheet: VSS) in FlowCAM system, and Equivalent Spherical Diameter (ESD) volume by the FlowCAM was used as a proxy for the estimation of phytoplankton biovolume. The ESD-based volume (V_{ESD}) is calculated based on the mean of 36 feret measurements which was conducted every 5° of specified directions

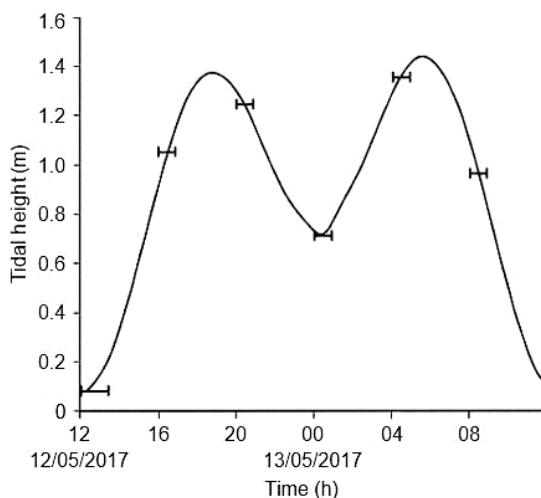


Fig. 2 Tide level (m) during the survey at Tatyama Bay, Japan. Bars represent start and end times of the samplings.

around the particle. Aggregate particles were checked and counted using VSS generated by the FlowCAM.

3. Results

3.1 Hydrological conditions (Figs. 3 and 4)

At 12 and 16 h, the upper layer (top 6 m) was heated by the solar radiation forming a certain gradient of water temperature (18.5–17.0 °C). The water column condition changed at 20 h, due to the intrusion of colder (15.5–13.5 °C) and saltier (34.4–34.6) water from the bottom during the flood. This intrusion mixed vertically the water column but was not strong enough to break the stratification up to the upper layer, forming a shallow layer thermocline at 1–6 m depth. At 00 h, when the water intrusion of the flood tide moved downward, and a thermocline was found at a deeper depth, 16–19 m with a temperature gradient (15.5–14.0 °C). At 04 h, the water column was well-mixed due to the high tidal current, and the colder and saltier water layer was located even deeper and almost not visible in our

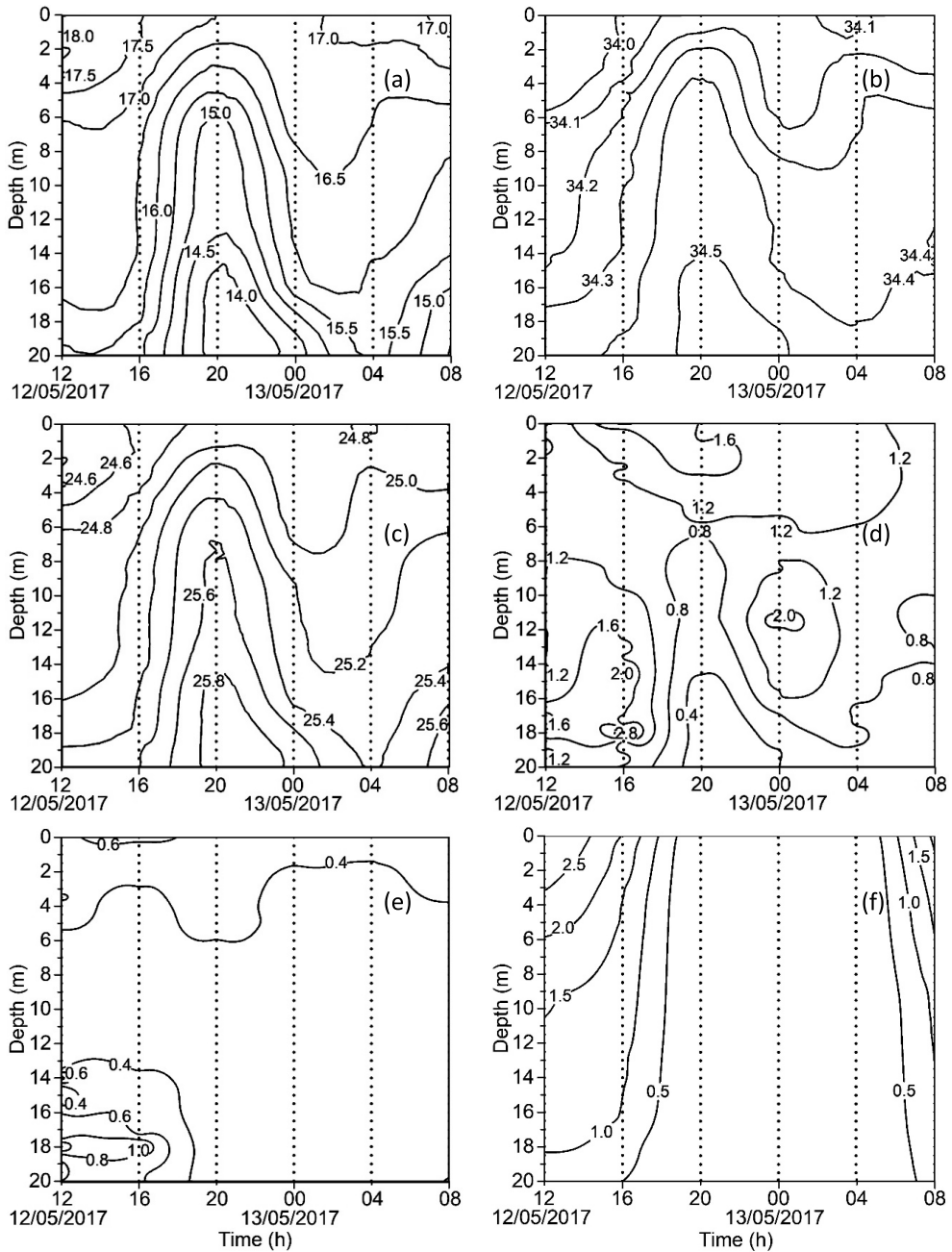


Fig. 3 Temporal changes in the vertical distribution of environmental properties on 12–13 May 2017. (a) water temperature ($^{\circ}\text{C}$), (b) salinity, (c) sigma- t , (d) Chl- a ($\mu\text{g L}^{-1}$), (e) turbidity (FTU), and (f) light intensity (PAR in $\log_{10} \mu\text{mol photons m}^{-2}\text{s}^{-1}$).

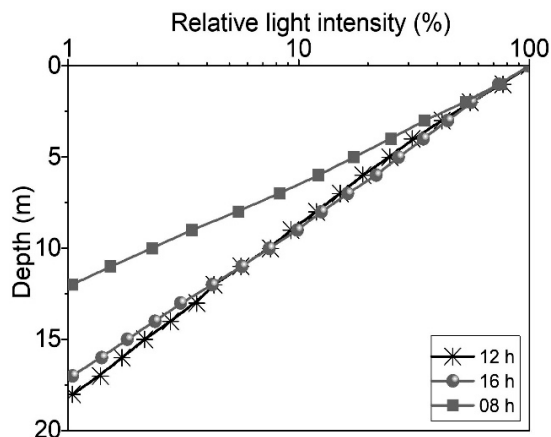


Fig. 4 Temporal changes in the vertical distribution of relative light intensity during 12–13 May 2017.

profiles. Later, at 08 h, the flood lifted this water mass again upwards, reaching the 16 m depth. At this time, the upper layer (0–14 m) remained well-mixed, showing a more homogeneous distribution of environmental parameters (Figs. 3a, b). The density profile showed the similar fluctuations governed by the temperature and salinity (Fig. 3c).

Regarding the chlorophyll-*a* fluorescence (Chl-*a*), the colder and saltier water found in the deeper layer that moved upwards during high tide showed distinctively low Chl-*a* (0.2–0.8 $\mu\text{g L}^{-1}$). Above this pool, typical peaks of Chl-*a* (1.6 and 3.1 $\mu\text{g L}^{-1}$) were observed at the bottom 18 m at 12 and 16 h, but at 20 h, peak (1.8 $\mu\text{g L}^{-1}$) moved to the upper layer 2.5 m, coincided with a thermocline, and then moved back to the deeper depth 11.5 m at 00 h, and disappeared in 04 and 08 h, respectively (Fig. 3d). Water turbidity was higher at 12 and 16 h, especially in the bottom layers where a significant increase in the Chl-*a* was noticed (Fig. 3e). The values of 1% I_0 depths (which indicate the bottom of the euphotic layer) in the day-time samplings were 18 m at 12 h, 17 m at 16 h and 12 m at 08 h, respec-

tively (Figs. 3f and 4).

3.2 Spatial and temporal distributions of total phytoplankton (Fig. 5)

At 12 h, phytoplankton distribution was heterogeneous with high densities 134 ± 13 cells mL^{-1} (mean \pm standard deviation) in the upper 0–4 m, and 115 ± 20 cells mL^{-1} at 7.5–20 m, respectively, and a low density 72 ± 26 cells mL^{-1} in the thermocline 4.5–7 m (Fig. 5a). At 16 h, phytoplankton showed a similar distribution pattern to that observed at 12 h, with high density 100 ± 13 cells mL^{-1} in the upper 4 m but decreased to 70 ± 9 cells mL^{-1} in the thermocline (4.5–7 m) and again an increasing trend 90 ± 19 cells mL^{-1} was observed below 7 m towards the bottom 20 m (Fig. 5b). Phytoplankton distribution pattern totally changed at 20 h, which was characterized by the formation of the pronounced thermocline at a shallow depth (1–6 m), where phytoplankton were concentrated 61 ± 21 cells mL^{-1} , but the distribution was restricted below the thermocline (Fig. 5c). At 00 h, thermal stratification in the upper layer was not seen, but it appeared in a deeper layer (16–19 m). At that time, phytoplankton were abundant (76 ± 11 cells mL^{-1}) above the thermocline at 9–14 m (Fig. 5d) and significantly decreased in the thermocline. The next samplings at 04 and 08 h, phytoplankton showed a rather homogeneous vertical distribution pattern in the water column (Figs. 5e, f), correspond with the effects of tidal mixing.

3.3 Phytoplankton assemblage composition (Table 1)

In our survey, a total of 22 phytoplankton taxa were identified, including 9 diatoms (Bacillariophyceae) such as *Thalassiosira* sp. (3,520 cells mL^{-1} , 27.5%), *Dactyliosolen fragilissimus* (1,776 cells mL^{-1} , 13.9%), *Pseudo-nitzschia* sp. (927

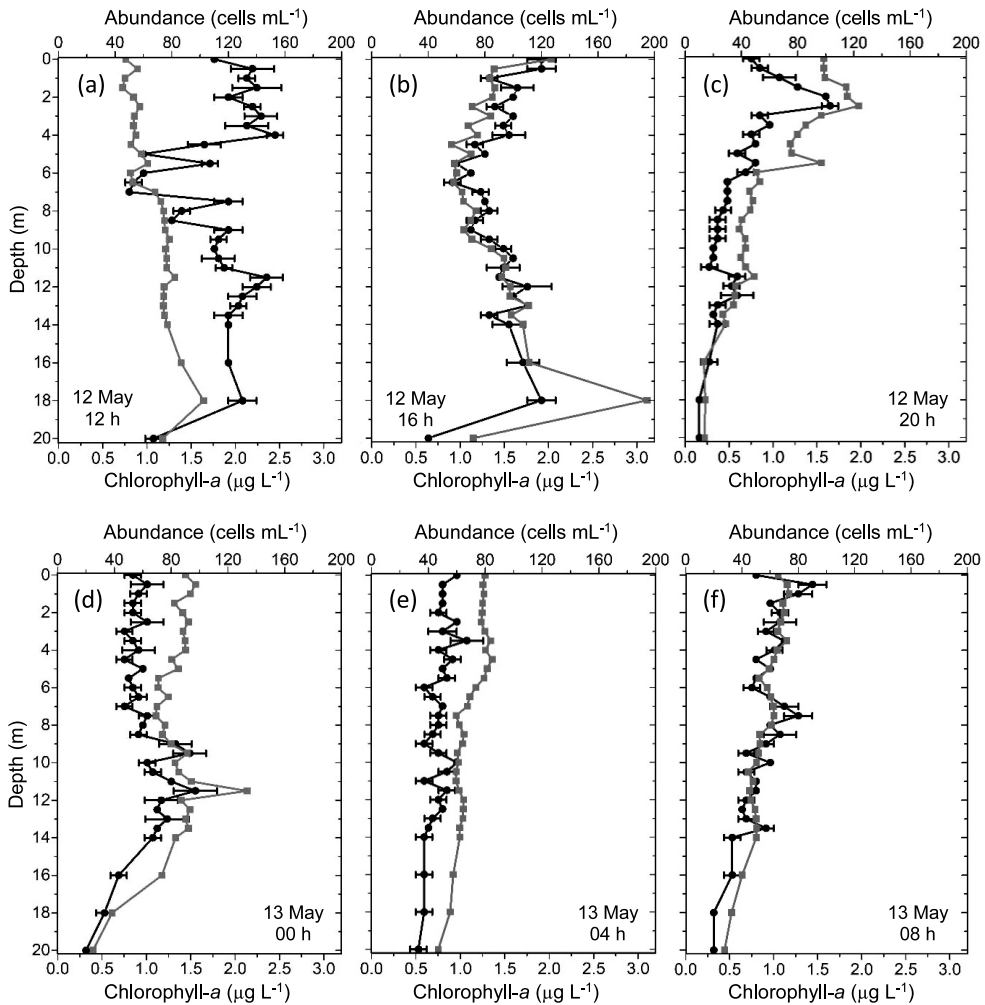


Fig. 5 Vertical distribution of total phytoplankton abundance for the six sampling times. Black line: average phytoplankton abundance, with standard deviation bar from the triplicate counts. Grey line: Chl-*a* concentration.

cells mL⁻¹, 7.2%), *Coscinodiscus* sp. (183 cells mL⁻¹, 1.4%), *Pleurosigma* sp. (49 cells mL⁻¹, 0.4%), *Lauderia annulata* (37 cells mL⁻¹, 0.3%), *Rhizosolenia setigera* (17 cells mL⁻¹, 0.1%), *Thalassionema nitzschioides* (13 cells mL⁻¹, 0.1%), and *Meuniera membranacea* (6 cells mL⁻¹, 0.05%); 10 dinoflagellates (Dinophyceae) such as *Prorocentrum minimum* (2, 622 cells mL⁻¹, 20.5%), *Scrippsiella trochoidea* (1,612 cells mL⁻¹,

12.6%), *Gyrodinium spirale* (501 cells mL⁻¹, 3.9%), *Protoperidinium quinquecorne* (253 cells mL⁻¹, 2.0%), *Heterocapsa* sp. (177 cells mL⁻¹, 1.4%), *Oxyphysis oxytoxoides* (76 cells mL⁻¹, 0.6%), *Ceratium furca* (23 cells mL⁻¹, 0.2%), *C. fusus* (7 cells mL⁻¹, 0.05%), *Gonyaulax spinifera* (10 cells mL⁻¹, 0.1%), and *Alexandrium* sp. (7 cells mL⁻¹, 0.05%); and other groups such as Raphidophyceae, Dictyochophyceae and Haptophy-

Table 1. List of phytoplankton in Tateyama Bay with total abundance, percentage, and average size (length and width).

Species	Total abundance		Length (μm)	Width (μm)
	cells mL^{-1}	%		
Bacillariophyceae				
<i>Coscinodiscus</i> sp.	183	1.4	50.0	37.7
<i>Dactyliosolen fragilissimus</i>	1,776	13.9	23.0	12.0
<i>Lauderia annulata</i>	37	0.3	23.7	16.9
<i>Meuniera membranacea</i>	6	0.05	57.8	31.1
<i>Pleurosigma</i> sp.	49	0.4	150.6	20.2
<i>Pseudo-nitzschia</i> sp.	927	7.2	30.3	4.6
<i>Rhizosolenia setigera</i>	17	0.1	379.0	5.2
<i>Thalassionema nitzschioides</i>	13	0.1	25.0	2.9
<i>Thalassiosira</i> sp.	3,520	27.5	18.9	12.5
Dinophyceae				
<i>Alexandrium</i> sp.	7	0.05	39.1	35.2
<i>Ceratium furca</i>	23	0.2	153.6	34.2
<i>Ceratium fusus</i>	7	0.05	343.7	30.5
<i>Gonyaulax spinifera</i>	10	0.1	29.6	23.1
<i>Gyrodinium spirale</i>	501	3.9	60.9	36.8
<i>Heterocapsa</i> sp.	177	1.4	30.7	21.1
<i>Oxyphysis oxytoxoides</i>	76	0.6	56.9	19.4
<i>Prorocentrum minimum</i>	2,622	20.5	22.2	18.5
<i>Protoperidinium quinquecorne</i>	253	2.0	23.7	18.7
<i>Scrippsiella trochoidea</i>	1,612	12.6	29.1	23.1
Dictyochophyceae				
<i>Dictyocha speculum</i>	10	0.1	29.5	21.3
Haptophyceae				
Coccolithophorid	468	3.7	13.2	12.3
Raphidophyceae				
<i>Heterosigma akashiwo</i>	303	2.4	29.8	24.3
Unidentified phytoplankton	205	1.5	13.9	11.9

ceae with only one species of each, *Heterosigma akashiwo* (303 cells mL^{-1} , 2.4%), *Dictyocha speculum* (10 cells mL^{-1} , 0.1%), and Coccolithophorid (468 cells mL^{-1} , 3.7%), respectively, and unidentified phytoplankton (205 cells mL^{-1} , 1.5%). Hence, the phytoplankton community was mainly dominated by diatoms and dinoflagellates (50%

and 42% of the total cell density).

Specifically, among these species, *Thalassiosira* sp., *D. fragilissimus*, *Pseudo-nitzschia* sp., *P. minimum*, and *S. trochoidea* were noted as the dominant species, which altogether contributed more than 80% of the total abundance of phytoplankton. Therefore, we consider their species-

specific distribution patterns in detail. The other species such as *L. annulata*, *Coscinodiscus* sp., *Rhizosolenia* sp., *T. nitzschioides*, *M. membranacea*, *Pleurosigma* sp., *G. spirale*, *Alexandrium* sp., *G. spinifera*, and *Heterocapsa* sp. were not observed in the colder and saltier water. Some dominant phytoplankton and the additional five species, *P. quinquecorne*, *O. oxytoxoides*, *C. furca*, *C. fusus*, and *D. speculum* that appeared after the high tide, only occurred in the colder and saltier water.

3.4 Species-specific distributions of dominant phytoplankton species (Fig. 6)

Thalassiosira sp. was numerically dominant throughout the study period and found at all sampling depths and times (Fig. 6a). *D. fragilissimus* distribution coincided with the thermocline, and they were trapped in the thermocline (1–6 m) at 20 h by the strong density gradients. Moreover, the cell density decreased to approximately the half (50%) after the high tide (18:20) and was not observed in the colder and saltier water mass (Fig. 6b). *Pseudo-nitzschia* sp. distribution pattern was not clear due to its low cell density throughout the sampling period (Fig. 6c). Similarly to *Thalassiosira* sp., *P. minimum* was detected at all sampling depths and times. An exception occurred at 20 h when a strong thermocline was marked at 1–6 m depth, where high cell densities were observed, but the distribution was limited below the thermocline (Fig. 6d). *S. trochoidea* distributed mainly in the first two samplings at 12 and 16 h; however, its distribution completely changed, and the abundance decreased to three-fourths (75%) after the high tide, 18:20 (Fig. 6e).

3.5 Phytoplankton biovolume versus Chl-*a* (Fig. 7)

At 12 and 16 h, the slope of the regression line

showed a negative correlation ($p > 0.05$), and an inverse relationship between the Chl-*a* and phytoplankton biovolume was observed (Figs. 7a, b). Thus, relatively low phytoplankton biovolume was found at a depth of Chl-*a* peak 18 m, where small-sized diatom, *Thalassiosira* sp. (Table 1) was dominant in those samples. At 20 h, a statistically positive correlation ($p < 0.05$) was seen between the Chl-*a* and biovolume. At that time, Chl-*a* peak occurred in the upper layer (1–6 m), where higher phytoplankton biovolume was observed (Fig. 7c). In the following sample at 00 h, Chl-*a* and biovolume showed a positive correlation due to the occurrence of large-sized dinoflagellates above the thermocline (9–14 m) where the Chl-*a* peak was detected (Fig. 7d). A positive relationship was detected between the Chl-*a* and biovolume for 04 and 08 h, respectively (Figs. 7e, f).

An allometric relationship of Chl-*a* with biovolume was found in most sampling times except for 12 and 16 h. At these times, the Chl-*a* peak was observed at the bottom layer where higher turbidity was recorded.

3.6 Vertical distribution of aggregate particles (Fig. 8)

Aggregates were generally more abundant in the first two samplings at 12 and 16 h (before high tide), especially at the bottom layers, with higher turbidity. After high tide (18:20), the formation of high abundance was not observed at the bottom in the following samplings at 20, 00, 04 and 08 h.

4. Discussion

Short-term phytoplankton dynamics are related to the changes of the water masses and hydrodynamic gradients such as stratification and mixing processes, influenced by the periodic oscillations of the tidal currents (BLAUW *et al.*,

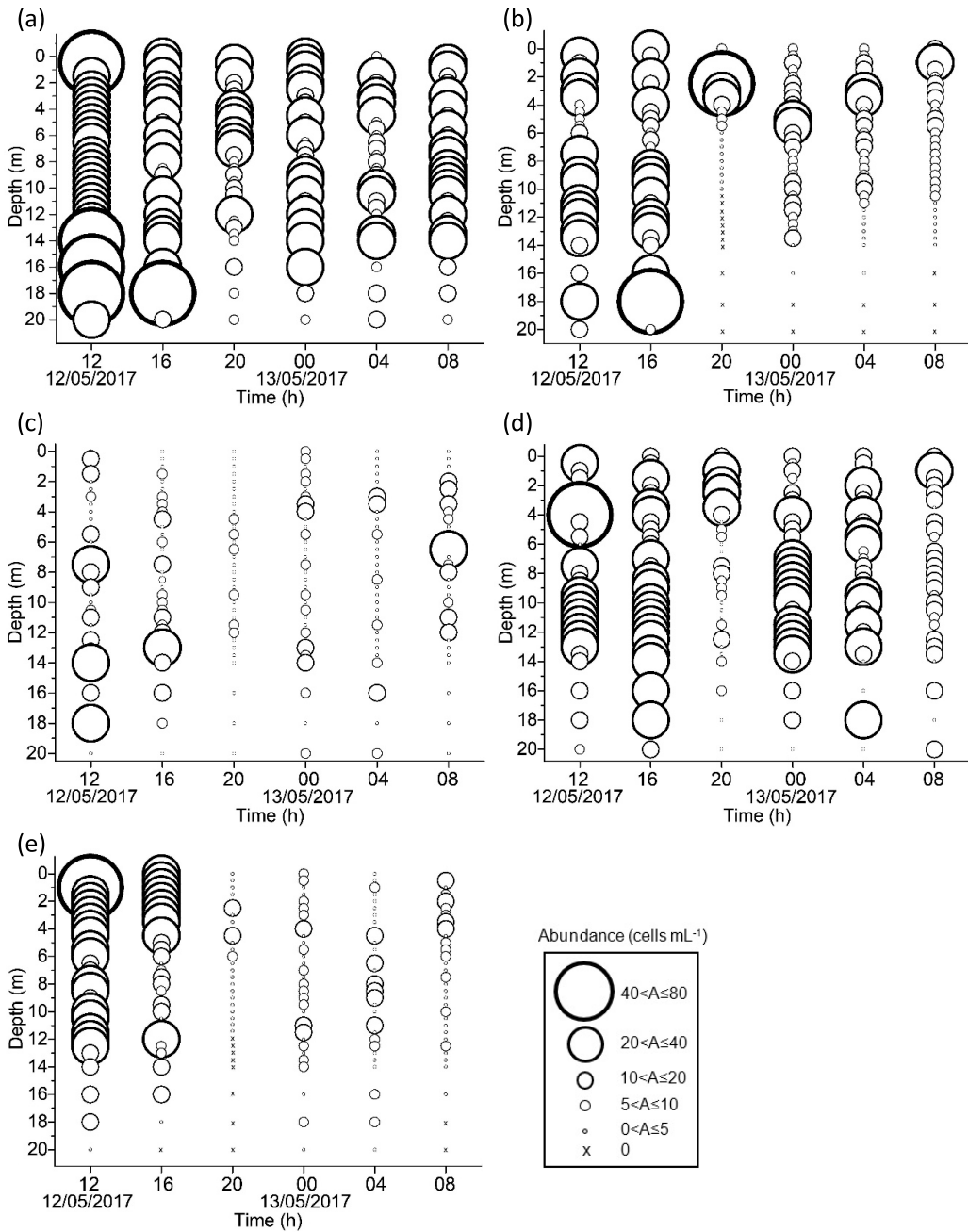


Fig. 6 Vertical distribution of dominant phytoplankton species (average of the six samplings): (a) *Thalassiosira* sp., (b) *Dactyliosolen fragilissimus*, (c) *Pseudo-nitzschia* sp., (d) *Prorocentrum minimum*, and (e) *Scrippsiella trochoidea*. "A" in the explanatory box represents "Abundance."

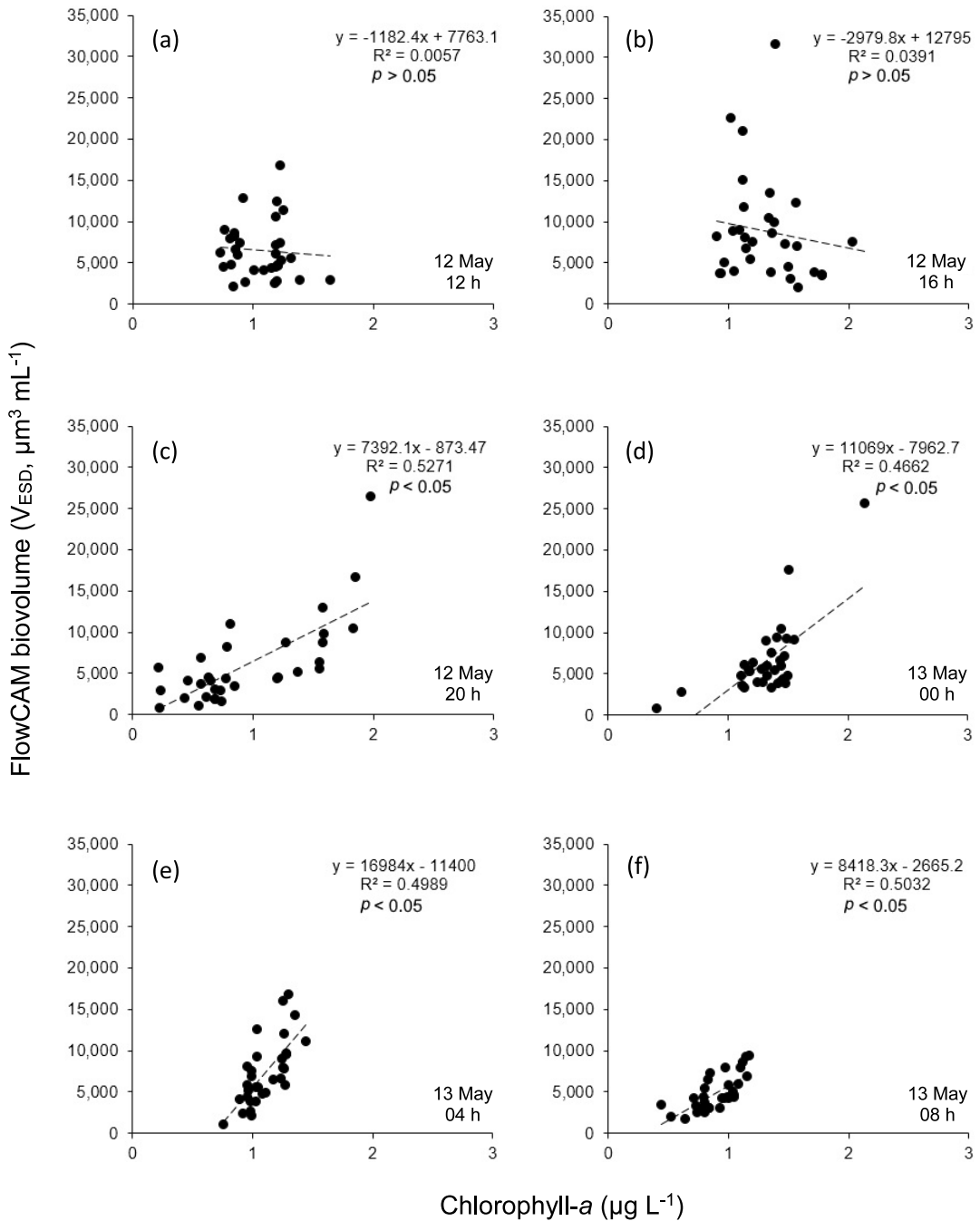


Fig. 7 Relationship between Chl-*a* and FlowCAM biovolume of total phytoplankton from the cell counts for 32 distinct vertical water layers ($n = 32$) during six sampling times. (a), (b), and (c) are for 12h, 16h, and 20h of 12 May; (d), (e), and (f) for 00h, 04h, and 08h of 13 May, respectively. The dashed line is fitted regression line.

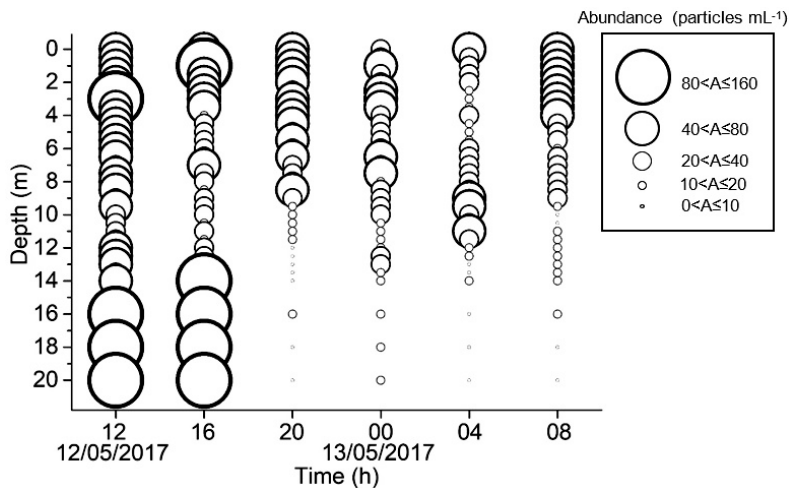


Fig. 8 Vertical distribution of aggregate abundance (average value of the triplicate analysis) for six sampling times. “A” in the explanatory box represents “Abundance.”

2012). During our study period, thermal stratification was likely to be influencing the spatial heterogeneity of phytoplankton distribution. Stratification was pronounced under weak tidal mixing condition. Temperature gradients then divided the water column into different strata by the density gradients that restricted the phytoplankton (but not entirely inhibit), resulting in a heterogeneous distribution. In contrast, it is likely that the vertical mixing generated by the tidal current homogenized the phytoplankton distribution in the water column. However, if tidal mixing was not strong enough, the water column could not be fully mixed, and stratification would remain in the upper layer. Thus, phytoplankton and Chl-*a* distributions differed among depths and sampling times due to the changes of the water masses and thermal structure.

In our study, both diatoms and dinoflagellates dominated the phytoplankton community. However, their composition to the phytoplankton community was different in the different layers and times, related with the changes of the water

mass structure, and probably the thickness of the euphotic layer. Changes were pronounced in the day-time at 12 and 16 h, when stratification of water mass force to form the diatoms and dinoflagellates aggregation in the water column. At these times, a large proportion of diatoms contributed to the phytoplankton community near the bottom where a high value of Chl-*a* was observed (Fig. 9a). In contrast, dinoflagellates were detected mainly in the upper water column coinciding with the thermocline but rarely observed in the deeper parts of the euphotic zone (Fig. 9b). This might be because the dinoflagellates prefer stratified water mass as has been explained in classical literatures (*e.g.* SMAYDA and REYNOLDS, 2001).

Thalassiosira sp. and *P. minimum* occurred at all sampling depths and times. These are euryhaline and eurythermal species, that are common in temperate coastal environments (POPOVICH and GAYOSO, 1999; HAJDU *et al.*, 2005). However, *D. fragilissimus* and *S. trochoidea* significantly decreased their abundance after the high tide,

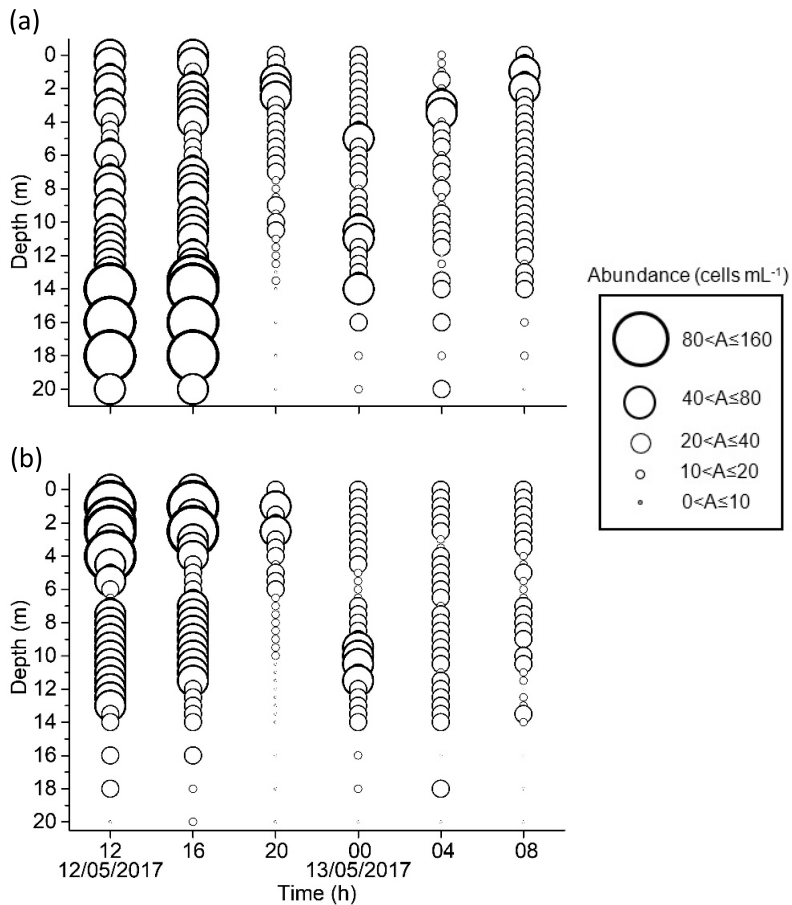


Fig. 9 Vertical distribution of (a): diatoms and (b): dinoflagellates abundance (average value of the triplicate analysis) for six sampling times. “A” in the explanatory box represents “Abundance.”

perhaps due to the changes of the water mass. During our survey, most phytoplankton species suddenly disappeared (except some dominant phytoplankton) after the high tide, when colder and saltier water mass intruded. It is suggested that these clear changes in species composition probably related to the changes of the water mass. Additionally, only five phytoplankton species, *P. quinquecorne*, *O. oxytoxoides*, *C. furca*, *C. fusus*, and *D. speculum* occurred in the colder and saltier water. Some of these five species (*C. furca* and *C. fusus*: Type VI (Coastal Entrained

Taxa)) were noted as the coastal habitat (SMAYDA and REYNOLDS, 2001).

Regarding the phytoplankton biovolume and Chl-*a*, a significant positive correlation was found in most sampling times except for 12 and 16 h. At these exceptional times, discrepancies were apparent because of the relatively low phytoplankton biovolume at a depth of Chl-*a* peak. In the case of 12 and 16 h, the water column was marked with a thermocline at 4.5–7 m depth, which may act as a barrier (SPRINTALL and CRONIN, 2001) between the upper and lower lay-

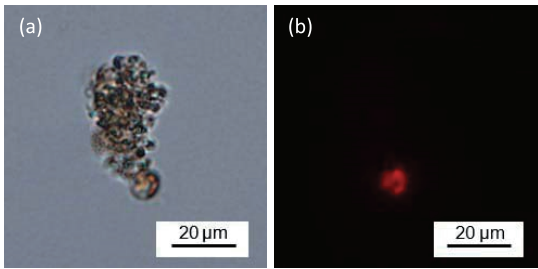


Fig. 10 Images of aggregates captured by an epi-fluorescence microscope using a fresh bottom sample obtained from Tokyo Bay as a trial. (a): bright field of aggregates, (b): fluorescence emits from aggregate under the dark field.

er. In the present study, the phytoplankton community in the lower layer was dominated by the smaller size phytoplankton species, such as *Thalassiosira* sp. and *D. fragilissimus*. Thus, phytoplankton biovolume was higher in the upper layer than those at a depth of Chl-*a* peak. Hence, a question rises “why Chl-*a* was high near the bottom?” We here speculate that the turbidity may be the key to answer this question because higher turbidity values coincided with the bottom Chl-*a* peaks. MATSUIKE *et al.* (1986) reported the increase of suspended particles in the water column is the major cause of water turbidity. This condition of high particle concentration leads to promote particle aggregation by colliding of smaller particles (JACKSON, 1990) or the release of phytoplankton structural bodies (ARMBRECHT *et al.*, 2004), or together with sediments, and detritus (ZIMMERMANN-TIMM, 2002).

Our vertical profile of the aggregates showed that the particle densities were higher in the bottom at 12 and 16 h, where the highly turbid water mass was observed. However, it was gone after the high tide, probably due to the intrusion of low turbidity water. At the same time, the Chl-*a* peak at the bottom disappeared, suggesting the relationship between the Chl-*a* and aggregate

particles. Hence, an additional experiment was done for the fluorescence analysis of the aggregates. Unfortunately, our formalin-fixed samples could not be used in the experiment, and thus we collected the fresh samples from the bottom water of Tokyo Bay while plankton survey cruising at the inner Tokyo Bay. From our observation with an epi-fluorescence microscope, emission of fluorescence was detected from the aggregates (Figs. 10a, b). This finding provides additional evidence for the consideration of Chl-*a* concentration in Tateyama Bay, which shows the high value at the bottom is not only from the phytoplankton but also from the fluorescence due to the pigments deposited in the aggregate particles that were floating there.

5. Conclusions

To assess the fine-scale spatio-temporal phytoplankton dynamics over a short time period, we used FlowCAM which can rapidly count, identify and size the phytoplankton. Our results indicated that phytoplankton distribution changed significantly in a short timescale (such as several hours) and in a few meters in depths, related with the eco-physiological characteristics of phytoplankton, the stratification and vertical mixing. Therefore, studies based on monthly or seasonal survey of phytoplankton with depth-averaged samplings may not well reveal the real community structure and the distribution patterns of phytoplankton that vary within a short time. Furthermore, our results showed that “Chl-*a*” does not always represent the phytoplankton abundance because it can be affected by detrital aggregate particles that contain a significant amount of fluorescent substances.

Acknowledgments

We thank the Laboratory of Aquatic Science Consultant Co., Ltd., which provided the use of a

FlowCAM and lab facilities. Sincere thanks are to the captain and crew members of T/R/V Seiyo-maru and students of Plankton Laboratory of Tokyo University of Marine Science and Technology, who helped the field sampling of significant difficulties. The present work was partially supported by the Monbukagakusho Scholarship for KKG., and also by JSPS KAKENHI Grant Numbers JP18H02263 for YT.

References

- ÁLVAREZ, E., M. MOYANO, Á. LÓPEZ-URRUTIA, E. NOGUEIRA and R. SCHAREK (2014): Routine determination of plankton community composition and size structure: a comparison between FlowCAM and light microscopy. *J. Plankton Res.*, **36**, 170–184.
- ARMBRECHT, L. H., V. SMETACEK, P. ASSMY and C. KLAAS (2004): Cell death and aggregate formation in the giant diatom *Coscinodiscus wailesii* (Gran & Angst, 1931). *J. Exp. Mar. Biol. Ecol.*, **452**, 31–39.
- BLAUW, A. N., E. BENINCÀ, R. W. P. M. LAANE, N. GREENWOOD and J. HUISMAN (2012): Dancing with the tides: fluctuations of coastal phytoplankton orchestrated by different oscillatory modes of the tidal cycle. *PLoS ONE*, **7**, e49319–e49319.
- CAMOYING, M. G. and A. T. YÑIGUEZ (2016): FlowCAM optimization: Attaining good quality images for higher taxonomic classification resolution of natural phytoplankton samples. *Limnol. Oceanogr.: Methods*, **14**, 305–314.
- CARON, D. A., B. STAUFFER, S. MOORTHY, A. SINGH, M. BATALIN, E. A. GRAHAM, M. HANSEN, W. J. KAISER, J. DAS, A. PEREIRA, A. DHARIWAL, B. ZHANG, C. OBERG and G. S. SUKHATME (2008): Macro-to fine-scale spatial and temporal distributions and dynamics of phytoplankton and their environmental driving forces in a small montane lake in southern California, USA *Limnol. Oceanogr.*, **53**, 2333–2349.
- DEKSHENIEKS, M. M., P. L. DONAGHAY, J. M. SULLIVAN, J. E. B. RINES, T. R. OSBORN and M. S. TWARDOWSKI (2001): Temporal and spatial occurrence of thin phytoplankton layers in relation to physical processes. *Mar. Ecol. Prog. Ser.*, **223**, 61–71.
- GAST, L., A. N. MOURA, M. C. P. VILAR, M. K. CORDEIRO-ARAÚJO and M. C. BITTENCOURT-OLIVEIRA (2014): Vertical and temporal variation in phytoplankton assemblages correlated with environmental conditions in the Mundaú reservoir, semi-arid northeastern Brazil. *Braz. J. Biol.*, **74**, 93–102.
- GERVAIS, F., U. SIEDEL, B. HEILMANN, G. WEITHOFF, G. HEISIG-GUNKEL and A. NICKLISCH (2003): Small-scale vertical distribution of phytoplankton, nutrients and sulphide below the oxycline of a mesotrophic lake. *J. Plankton Res.*, **25**, 273–278.
- HAJDU, S., S. PERTOLA and H. KUOSA (2005): *Prorocentrum minimum* (Dinophyceae) in the Baltic Sea: morphology, occurrence- a review. *Harmful Algae*, **4**, 471–480.
- HARRIS, R. P., L. FORTIER and R. K. YOUNG (1986): A large-volume pump system for studies of the vertical distribution of fish larvae under open sea conditions. *J. Mar. Biol. Ass. U. K.*, **66**, 845–854.
- ITOH, H., A. TACHIBANA, H. NOMURA, Y. TANAKA, T. FUROTA and T. ISHIMARU (2011): Vertical distribution of planktonic copepods in Tokyo Bay in summer. *Plankton Benthos Res.*, **6**, 129–134.
- JACKSON, G. A. (1990): A model of the formation of marine algal flocs by physical coagulation processes. *Deep-Sea Res.*, **37**, 1197–1211.
- JAPAN METEOROLOGICAL AGENCY WEBSITE (2017): http://www.data.jma.go.jp/kaiyou/data/db/tide/suisan/pdf_hourly/2017/TT.pdf.
- LUNVEN, M., J. F. GUILLAUD, A. YOUÉNOU, M. P. CRASSOUS, R. BERRIC, E. LE GALL, R. KÉROUEL, C. LABRY and A. AMINOT (2005): Nutrient and phytoplankton distribution in the Loire River plume (Bay of Biscay, France) resolved by a new Fine Scale Sampler. *Estuar. Coast. Shelf Sci.*, **65**, 94–108.
- MATSUIKE, K., T. MORINAGA and T. HIRAOKA (1986): Turbidity distributions in Tokyo Bay and movement of the turbid water. *J. Tokyo Univ. Fish.*, **73**, 97–114.
- MAZNAH, W. O. W., S. RAHMAH, C. C. LIM, W. P. LEE, K. FATEMA and M. M. ISA (2016): Effects of tidal events on the composition and distribution of

- phytoplankton in Merbok river estuary Kedah, Malaysia. *Trop. Ecol.*, **57**, 213-229.
- MELLARD, J. P., K. YOSHIYAMA, E. LITCHMAN and C. A. KLAUSMEIER (2011): The vertical distribution of phytoplankton in stratified water columns. *J. Theor. Biol.*, **269**, 16-30.
- POPOVICH, C. A. and A. M. GAYOSO (1999): Effect of irradiance and temperature on the growth rate of *Thalassiosira curviseriata* Takano (Bacillariophyceae), a bloom diatom in Bahía Blanca estuary (Argentina). *J. Plankton Res.*, **21**, 1101-1110.
- POULTON, N. J. and J. L. MARTIN (2010): Imaging flow cytometry for quantitative phytoplankton analysis - FlowCAM. *In* Microscopic and Molecular Methods for Quantitative Phytoplankton Analysis. KARLSON, B., C. CUSACK and E. BRESNAN (eds.), UNESCO (IOC Manuals and Guides, no. 55.), Paris, p. 47-54.
- SEE, J. H., L. CAMPBELL, T. L. RICHARDSON, J. L. PINCKNEY and R. SHEN (2005): Combining new technologies for determination of phytoplankton community structure in the northern Gulf of Mexico. *J. Phycol.*, **41**, 305-310.
- SIERACKI, C. K., M. E. SIERACKI and C. S. YENTSCH (1998): An imaging in-flow system for automated analysis of marine microplankton. *Mar. Ecol. Prog. Ser.*, **168**, 285-296.
- SMAYDA, T. J. and C. S. REYNOLDS (2001): Community assembly in marine phytoplankton: application of recent models to harmful dinoflagellate blooms. *J. Plankton Res.*, **23**, 447-461.
- SPRINTALL, J. and M. F. CRONIN (2001): Upper ocean vertical structure. *In* Encyclopedia of Ocean Science. STEELE, J. H., S. A. THORPE and K. K. TUREKIAN (eds.), Academic Press, San Diego, p. 3120-3129.
- TAUXE, L., J. L. STEINDORF and A. HARRIS (2006): Depositional remanent magnetization: Toward an improved theoretical and experimental foundation. *Earth Planet. Sci. Lett.*, **244**, 515-529.
- TILZER, M. M. and C. R. GOLDMAN (1978): Importance of mixing, thermal stratification and light adaptation for phytoplankton in Lake Tahoe (California, Nevada). *Ecology*, **59**, 810-821.
- ZIMMERMANN-TIMM, H. (2002): Characteristics, dynamics and importance of aggregates in rivers - An invited review. *Int. Rev. Hydrobiol.*, **87**, 197-240.

Received: 26 April, 2019

Accepted: 6 August, 2019